Original Article

Aneuploid IMR90 cells induced by depletion of pRB, DNMT1 and MAD2 show a common gene expression signature

Danilo Cilluffo[a], Viviana Barra[a,1], Sergio Spatafora[a], Claudia Coronnello[b], Flavia Contino[a], Serena Bivona[a,d], Salvatore Feo[a,d], Aldo Di Leonardo[a,c,*]

[a] Department of Biological, Chemical and Pharmaceutical Sciences and Technologies, University of Palermo, Italy
[b] Fondazione Ri.MED, Palermo, Italy
[c] Centro di OncoBiologia Sperimentale (COBS), Palermo, Italy
[d] Advanced Technology Network Center (ATEN), University of Palermo, Italy

A R T I C L E   I N F O

A B S T R A C T

Chromosome segregation defects lead to aneuploidy which is a major feature of solid tumors. How diploid cells face chromosome mis-segregation and how aneuploidy is tolerated in tumor cells are not completely defined yet. Thus, an important goal of cancer genetics is to identify gene networks that underlie aneuploidy and are involved in its tolerance. To this aim, we induced aneuploidy in IMR90 human primary cells by depleting pRB, DNMT1 and MAD2 and analyzed their gene expression profiles by microarray analysis. Bioinformatic analysis revealed a common gene expression profile of IMR90 cells that became aneuploid. Gene Set Enrichment Analysis (GSEA) also revealed gene-sets/pathways that are shared by aneuploid IMR90 cells that may be exploited for novel therapeutic approaches in cancer. Furthermore, Protein-Protein Interaction (PPI) network analysis identified TOP2A and KIF4A as hub genes that may be important for aneuploidy establishment.

1. Introduction

Aneuploidy is characterized by an unbalanced number of chromosomes (whole-chromosome aneuploidy) or by the rearrangement of large portions of chromosomes (Segmental aneuploidy). Segmental aneuploidy refers to chromosomal rearrangements (*deletions, inversions, translocations),* which arise from DNA breaks, and alters the copy number of many genes. Similarly, whole-chromosome aneuploidy modifies genes' copy number but originates from errors in chromosome segregation occurring in mitosis. Cells are provided with a surveillance system, the Spindle Assembly Checkpoint (SAC), that generally safeguards chromosome stability by preventing anaphase onset until all sister chromatids are properly attached (amphitelic attachment) to the mitotic spindle [1]. A weakened SAC, could then promote aneuploidy that is a major feature of virtually all solid tumors. Aneuploidy in cancer cells could also be responsible for the acquisition of favorable mutations that allow those cells to escape stringent growth control and become drug resistant [2]. Despite its close connection to cancer, the genomic imbalance caused by aneuploidy has been shown to reduce cellular fitness and inhibit growth of diploid cells in a variety of model systems [3,4]. Both trisomic Mouse Embrionic Fibroblasts (MEFs) and

disomic yeast laboratory strains showed increased doubling times when compared to their diploid counterparts [5,6]. Accordingly, MEFs with induced trisomy or tetrasomy and cancer cell with Chromosome Instability (CIN) exhibit specific anti-proliferative transcriptional profiles [7,8]. These negative effects were attributed to a 'proteotoxic stress' caused by an unbalanced expression of proteins, one of the consequences of altered gene copy number [9,10]. Growth defects in aneuploid laboratory yeast and human aneuploid cells were associated with the induction of Environmental Stress Response genes (ESR) and stress response, respectively [11–14]. However, the low rate of growth defects observed in aneuploid wild yeasts in the absence of ESR induction, and the display of different transcriptional programs seen in human aneuploid tumors, suggest the existence of gene networks that confer aneuploidy tolerance [15]. How diploid cells deal with chromosome mis-segregation and how aneuploidy is tolerated in tumor cells has not been completely understood yet. Moreover, one aneuploidy-tolerating mechanism that has been suggested is the enhanced proteasomal degradation [9,16,17]. Also, dysfunction of the p38-p53 axis was suggested to promote proliferation of aneuploid human tumor cells [18]. Recently, we showed that p14^{ARF}-mediated p53 stabilization induced premature cellular senescence to block the deleterious effects of

* Corresponding author at: Dipartimento STEBICEF, University of Palermo, viale delle Scienze, 90128 Palermo, Italy.
  E-mail address: aldo.dileonardo@unipa.it (A. Di Leonardo).
[1] Present address: Department of Genetic Stability and Oncogenesis, CNRS UMR8200, Institut Gustave Roussy, 94805 Villejuif, France.

aneuploidy in primary human cells [19] and that ectopic expression of p14[ARF] induced p53-dependent apoptosis [20]. These findings suggest that cancer cells have acquired the ability to overcome these barriers. The occurrence of aneuploidy in cancer cells is best explained as a combination of mitotic errors and an elevated tolerance to whole chromosome gains and losses caused by aneuploidy-tolerating mutations in tumor cells [21]. Thus, a major goal of cancer genetics is the identification of mutated genes and altered pathways leading to chromosome instability/aneuploidy, and of gene networks conferring tolerance for aneuploidy in cancer cells.

Our published data and those from other laboratories have shown that depletion of MAD2 [19], pRB [22], DNMT1 [23], triggered aneuploidy, suggesting that commonly deregulated genes/pathways underlie aneuploidy. However, we still lack complete knowledge of specific gene/s network/s that are responsible for: *i.* triggering aneuploidy, *ii.* inducing aneuploidy tolerance.

By high-throughput gene expression profiling using microarrays analysis, we identified genes/pathways altered in human primary fibroblasts in which aneuploidy was induced by posttranscriptional silencing of RB, DNMT1 and MAD2 genes. Bioinformatic analysis suggested the existence of a shared gene expression signature in response to aneuploidy. This expression profile can be useful to investigate into the deregulated pathways that are common to aneuploid cells.

2. Results

2.1. Depletion of DNMT1, MAD2 and pRB induces aneuploidy in IMR90 primary human fibroblasts

To differentially induce aneuploidy in otherwise diploid human primary fibroblasts (IMR90) we depleted pRB, DNMT1 and MAD2. We first determined the optimal siRNA concentration able to reduce the targeted transcripts without affecting cell viability. To this end, different concentrations of siRNAs (40 nM, 60 nM and 80 nM) were tested to establish the correct amount of siRNA to deplete DNMT1, MAD2 and pRB and capable to induce aneuploidy in 72 h. In order to avoid cytotoxic effects caused by complete MAD2 depletion [24], we used a concentration of siRNA (60 nM) lower than the one used to deplete DNMT1 and pRB (80 nM). By using the 60 nM concentration of siRNA to target MAD2 it was possible to mimic the haplo-insufficient condition (presence of about 50% of mRNA) as showed in Fig. 1A. Western blot analysis after 72 h from siRNAs treatment showed that RNAi induced a specific decrease of the target proteins in each sample (Fig.1B).

As expected, the depletion of DNMT1, MAD2 and RB caused the increase in the number of aneuploid cells (Fig. 2) in respect to that detected in IMR90 cultured cells [25].

We then performed cytogenetic analysis and counted the number of chromosomes per metaphase spread. The number of aneuploid cells was assessed by conventional cytogenetics by observing metaphase spreads 72 h post-transfection of specific siRNAs. Moreover, aneuploidy in the depleted cells was confirmed by Fluorescence in situ Hybridization on
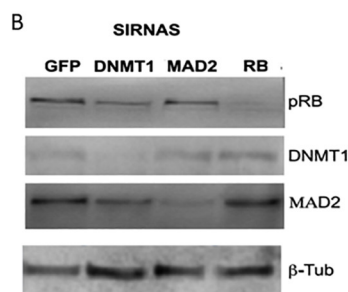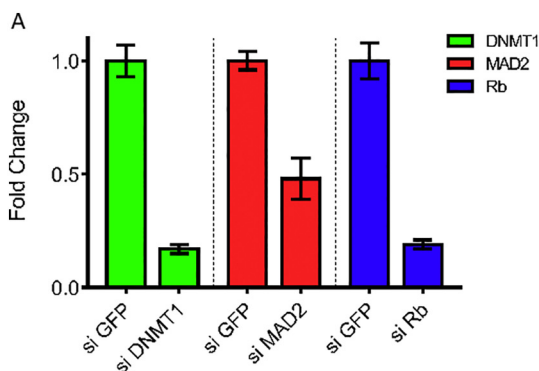
interphase nuclei (iFISH) using specific alphoid probes detecting chromosomes #6, #7, #8 and #17, respectively. Interphase FISH analysis detected nuclei in which chromosomes deviate from the modal number of two (Fig. 3). The number of these aneuploid cells increased by 2–5% for each chromosome-specific probe analyzed when compared to the control (siGFP).

2.2. Transcriptome and bioinformatic analyses

We analyzed transcriptome changes by microarray analysis following 72 h after RNA interference of DNMT1, MAD2 and pRB in IMR90 cells to gain evidence of a putative common molecular signature shared by the differently induced aneuploid cell populations. This approach of whole genome expression analysis could suggest the existence

Fig. 2. RNA interference of DNMT1, RB and MAD2 induces aneuploidy and does not affect the proliferation. (A) The graph summarizes the results of conventional cytogenetic analysis of IMR90 cells after 72 h from transfection with the indicated siRNAs. IMR90 cells transfected with the siRNA targeting the Green Fluorescent Protein (siGFP) were used as a control. (B) Histogram showing the proliferation rate of the indicated samples.

Fig. 1. Post-transcriptional silencing of DNMT1, RB and MAD2. (A) Quantitative Reverse transcription PCR (RT-qPCR) showing mRNA reduction in IMR90 cells following 72 h of RNAi of DNMT1, RB and MAD2. The siRNA specific for the GFP gene was used as a control. (B) Western blot showing the amount of the indicated protein after RNAi.
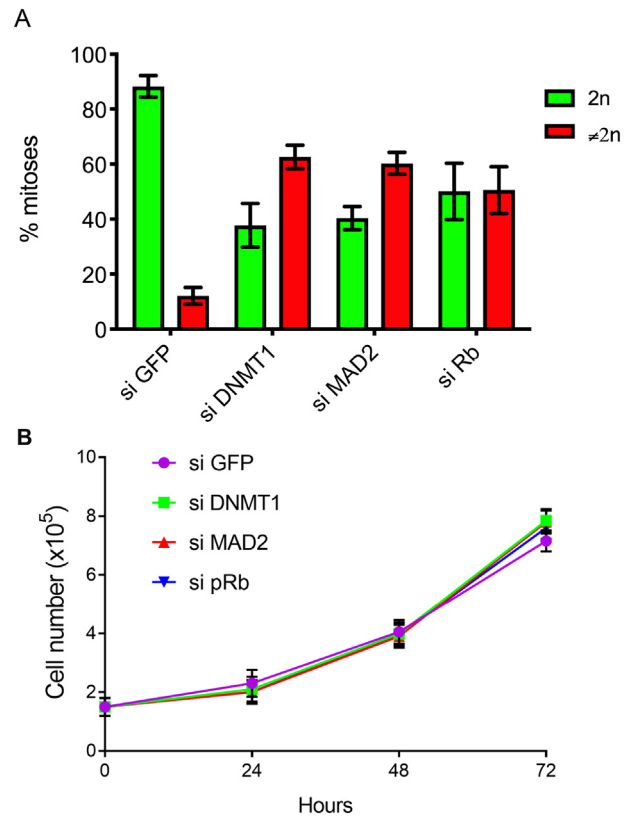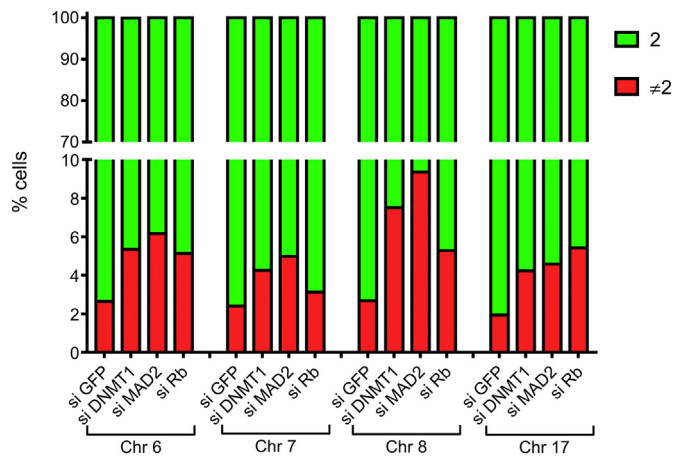
Fig. 3. Aneuploidy detected in interphase nuclei by Fluorescence in situ Hybridization (iFISH). Detection by iFISH of aneuploidy occurrence as revealed by the deviation from the modal chromosome number (two) for chromosome # 8, 7, 6, 17, in depleted human primary fibroblasts (IMR90).

of gene network/s underlying aneuploidy. The microarray analysis included two groups with six replicates (siDNMT1 and sipRB) and two groups with five replicates (siMAD2 and siGFP). The hierarchical clustering dendrogram comparing IMR90 cells transfected with siGFP (control) and siRNA against the three selected genes is shown in Fig. 4A. To identify the differentially expressed genes' (DEGs) probe-sets, data from replicate experiments were merged, and each expression profile was collated by gene name and filtered by the databases' annotated genes. DEGs with a significance level of $p < .05$ and a fold change > 1.5 were selected. This process resulted in 768 DEGs in IMR90-siDNMT1 (475 upregulated, 311 downregulated), 1313 DEGs in IMR90-siMAD2 (725 upregulated, 588 downregulated) and 1958 in IMR90-sipRB (1317 upregulated, 641 downregulated). Finally, we observed that from the data obtained with the 41,000 probe-sets represented in the arrays, 4039 genes were significantly differentially expressed (2353 upregulated and 1686 downregulated). More details can be found in Supplementary material S1.

A Gene Ontology (GO) (www.Geneonthology.org) analysis of the identified 4039 DEGs was performed using FunRich V3 [26]. Fifteen Molecular Functions (MF) terms were found significantly enriched, including DNA and Chromatin binding, Protein serine/threonine kinase and phosphatase activities and transcription regulator activity. In addition, five Cellular Component (CC) terms were found significantly enriched, including Nucleus, Kinetochore and Chromosome. Also, nine terms were found significantly enriched among the Biological Process including Regulation of Nucleic Acid Metabolism, Cell Cycle and Chromosome segregation (detailed results are reported in Supplementary material S2). DEGs were also grouped according to their involvement in specific pathways. The result of this mapping (Fig. 4B) highlights a set of genes mainly involved in the ATM pathway, the Cell Cycle, the Mitotic pathway, and the Mitotic M/G1 and Mitotic G1/S phases (detailed results are reported in Supplementary material S2).

Finally, we identified DEGs that are common to IMR90 cells after depletion of DNMT1, MAD2 and pRB (Fig. 4C). Sixty-five (48 upregulated and 17 downregulated) annotated DEGs that are coordinately expressed (heat map in Fig. 4D and Supplementary material S1), were shared by the three samples. Among the un-shared DEGs we observed a significant down-regulation of the targeted genes: DNMT1 (FC-4.16, *p*-value 3.3 × 10^{-4}), MAD2 (FC -6.63, *p*-value 3.3 × 10^{-7}) and RB (FC -4.10, *p*-value 4.2 × 10^{-11}), strongly supporting the reliability of our microarray analysis.

2.3. Validation of arrays data using RT-qPCR analysis

We further validated the observed gene expression changes found with the microarray analysis by RT-qPCR in independent biological replicates of IMR90 cells treated with the different siRNAs under the same conditions used for the microarrays. Seven upregulated common DEGs were selected for RT-qPCR analysis: EGFR, FAM3C, IGFBP1, MARCH4, NAP1L5, SCLY and SERTAD2 (Fig. 5). Gene fold changes resulting from RT-qPCR were mostly in agreement with the microarray data (data not shown). Although there was a small difference in the fold change value between the two methods, the results generally were highly correlated (Sperman's rank correlation coefficients were 0.6680, 0.8571 and 0.5740 for siDNMT1, MAD2 (MAD2L1) and pRB (RB1), respectively, with two-tailed *p*-values ranging from 0.023 to 0.001).

2.4. Gene set enrichment analysis (GSEA) analysis

Normalized data were also analyzed with the GSEA web-tool (www.broadinstitute.org/gsea) to detect the pathways/gene-sets significantly deregulated in each treatment (sipRB, siMAD2, siDNMT1) with respect to the control (siGFP). This analysis revealed unique (Supplementary material S3) and common pathways altered in aneuploid human fibroblasts. Table 1 shows the significant (*p* value < .005) common deregulated GSEA Gene-Sets and associated DEGs.

By bioinformatics it was possible to list several DEGs and then generate a sub-list of common pathways and regulatory factors. The common molecular signature in all aneuploid cell lines analyzed is characterized by deregulation of the following Gene Sets: *Mitotic Spindle, G2M Checkpoint, E2F Targets, MYC Targets V2* (A subgroup of genes regulated by MYC) and *P53 Pathway* (Table 1).

We found twenty-nine downregulated genes belonging to the *Mitotic Spindle* gene-set that were shared among the three samples (Fig. 6). Among these, eight are mitotic spindle associated genes (CENP-E, KIF23, KIF11, KIF4A, RAKGAP1, ESPL1, TPX2, NIN) and three are SAC genes (TTK, BUB1, PLK1). We found seventeen upregulated genes belonging to the *P53 Pathway* gene-set and shared among all samples (Fig. 6), in particular, four of these genes (BTG2, FDXR, DDB2, FBXW7) are transcriptional targets of p53 [27]. The remaining three gene-sets, the *G2M Checkpoint*, the *E2F Targets* and *MYC Targets V2*, seem to be differently deregulated in all samples. Specifically, the G2M Checkpoint and E2F Targets were downregulated in siMAD2 and siDNMT1 samples and upregulated in the siRB sample, whereas MYC Targets V2 were downregulated in siDNMT1 sample and upregulated in siMAD2 and siRB samples.

2.5. PPI network analysis

The PPIs among the proteins encoded by the 66 common DEGs identified by the GSEA method were predicted using STRING. The constructed network consisted of 62 proteins (nodes) and 226 interactions (edges) (Fig. 7A). In addition, there were five genes that were highly connected with edges ≥15 in the PPI network. These five genes were TOP2A (21 edges), KIF2C (18 edges), KIF4A (18 edges), RACGAP1 (18 edges) and TTK (16 edges). ClusterONE was applied for module analysis to further predict potential protein complexes. For the network described above, there were two significant modules with *p*-value < .0005: one module shown in Fig. 7B (nodes, 16; density, 0.361; quality, 0.580; *p*-value = 1.319 × 10^{-7}) where TOP2A protein is seen as the most connected, and one module shown in Fig. 7C (nodes, 14; density, 0.291; quality, 0.453; *p*-value = 7.759 × 10^{-7}), where KIF4A protein is seen as the most connected.

3. Discussion

Several negative features have been associated to the aneuploidy phenotype in eukaryotes such as developmental defects, alterations of
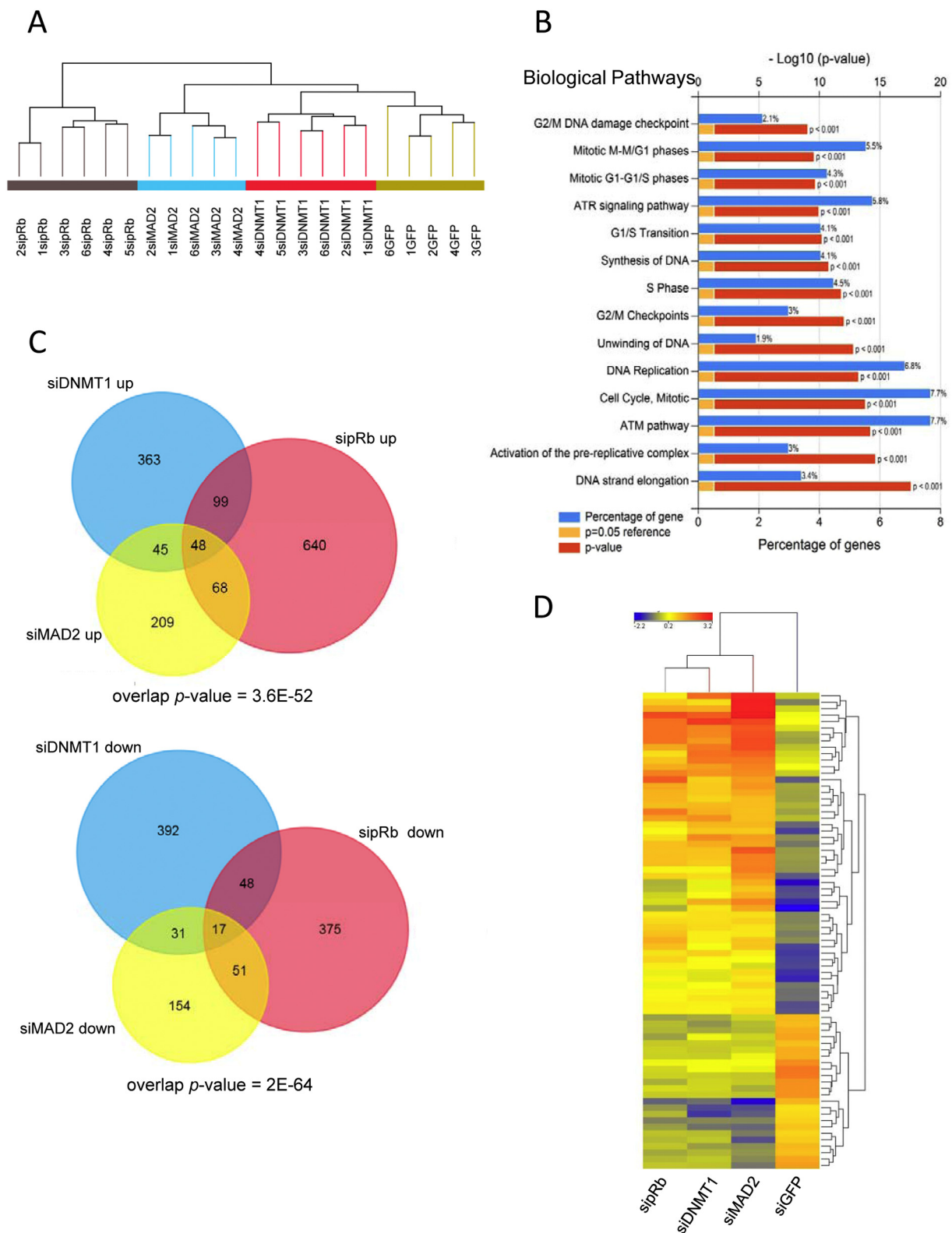
Fig. 4. Comprehensive gene expression analysis in sipRB, siDNMT1 and siMAD2 transfected IMR90 cells. (A) Unsupervised hierarchical clustering dendrogram, based on 4039 differentially expressed and filtered probe-sets (FC ± 1.5, *p*-value cutoff ≤0.05), comparing IMR90 cells transfected with siGFP (control) and siRNA targeting pRB, MAD2 and DNMT1. (B) Biological pathways for DEGs. X axis represent percentage of genes or –log10(*p*-value); Y axis represent the Biological pathways found significantly enriched using the FunRich database [26]. (C) Venn diagram showing the number of unique and common up- and down-regulated DEGs found in the indicated partially depleted *IMR90* cells (see Supplementary material S1). Overlap *p*-value was computed by using the Hypergeometric distribution, implemented by the phyper function in R. (D) Heat map showing transcription fold changes of significantly altered DEGs in RNA interfered IMR90 cells. Each row represents a single gene, a list of the genes and associated fold change is available in Supplementary material S1.
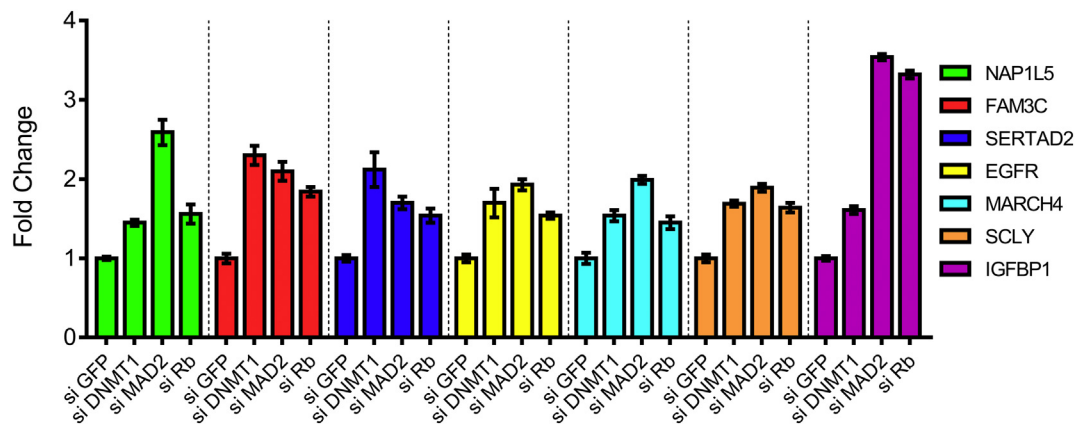
Fig. 5. Relative mRNA expression levels of specific genes in different groups of siRNA transfected IMR90 cells. Quantitative reverse transcription PCR (RT-qPCR) results from siDNMT1, siMAD2 and sipRB transfected IMR90 cells, compared to siGFP transfected cells. The assays were performed in quadruplicates and repeated in three independent experiments. The data are presented as the mean ± SD (error bar) of fold-change.

protein homeostasis, genetic instability and reduced fitness of diploid cells. A weakened Spindle Assembly Checkpoint (SAC) can promote aneuploidy and thus, trigger cancer transformation. One example is BubR1 mutation, a SAC component, that generates the Mosaic Variegated Aneuploidy (MVA) disease associated with early cancer development [28]. In addition, mice that are heterozygous for Centromere Protein E (CENPE) exhibit whole chromosome aneuploidy associated with the increase of spontaneous tumors [29]. Thus, aneuploidy can confer to cancer cells the ability to overcome the proliferation barriers. Aneuploidy tolerance, driven by aneuploidy associated gene imbalance or by additional mutations, should accompany tumorigenesis. We generated three aneuploid model cell populations by post-transcriptional silencing of pRB, DNMT1 or MAD2 genes for 72 h and analyzed their gene expression profiles by microarray. A detailed bioinformatics gene expression analysis (GSEA) showed gene expression profiles in response to aneuploidy in human primary cells. The "Mitotic Spindle" gene-set was found altered in all three samples suggesting that downregulation of genes belonging to this gene-set is necessary for the survival of cells prone to chromosome missegregation after triggering aneuploidy. The *P53 Pathway* gene-set was upregulated in all three samples, which suggests a common response to the stress caused by chromosomal imbalance. Interestingly, the BTG2 gene, belonging to this gene-set, is an antiproliferative factor induced by p53/NF-kB signalling in response to a variety of genotoxic and cellular stress (DNA damage, hypoxia, etc.) [27]. Our finding that BTG2 is overexpressed in induced aneuploid IMR90 cells suggests a possible protective role of BTG2 in response to aneugenic triggers. In fact, its downregulation has been shown to be implicated in cell transformation, epithelial to mesenchymal transition and cancer progression [30]. Unlike the latter two pathways, found equally altered in all samples, the *G2M Checkpoint*, *E2F Targets* and *MYC Targets V2* gene-sets turned out to be differently deregulated in the three samples. In particular the *G2M*

Checkpoint and *E2F Targets* gene-sets resulted in a downregulation in siMAD2 and siDNMT1 samples and an upregulation in the siRB sample. On the contrary, the *MYC Targets V2* -gene-set resulted in a downregulation in the siDNMT1 sample and an upregulation in the siMAD2 and siRB samples. In addition, we found that MCM2, MCM6 and MCM7 genes, components of the MCM (Mini Chromosome Maintenance) complex, are downregulated in aneuploid human fibroblasts induced by DNMT1 and MAD2 depletion. The MCM family of genes were originally identified as factors required for minichromosome maintenance in yeast models, thus reduction of MCMs may be aneuploidogenic additionally [32]. MCM2 decrease has been reported as a consequence of chromosome mis-segregation (polyploidy) caused by EG5 inhibition in SAC impaired Hela cells [31]. Downregulation of all of the subunits of the replicative helicase complex MCM2-7 have been observed in trisomic and tetrasomic HCT116 and RPE1 cells and it was suggested to explain the aneuploid-induced genomic instability (GIN) [33]. In addition, replication stress and genomic instability following chromosome missegregation was considered the trigger for cells with harbouring numerical and segmental aneuploidies [34]. Thus, MCMs downregulation might cause replication stress and genomic instability in human cells. Differently from what observed in the transgenic CIN mouse model (Shugoshin1$^{-/+}$) [35,36] our aneuploid cells populations did not show shared altered pathways relative to immune response, lipid metabolism or stem cells regulation, though they exhibit such deregulations as single samples (Supplementary material S3). This could suggest that the common first steps of the aneuploid phenotype acquisition modulate biological processes that are cell-related (i.e. cell cycle checkpoints and chromosome segregation) rather than tissue/organism related.

Interestingly, although the same pathway is deregulated in our individual aneuploid populations, the genes with altered expression are often variable, suggesting that the induction and likely the maintenance of aneuploidy rely mainly on the alteration(s) of a pathway(s) rather

Table 1
Gene sets shared by DNMT1/MAD2/pRB partially depleted cells.

| Hallmark gene sets	No. of genes in the dataset				
	siMAD2	siDNMT1	sipRB	Common	Genes
MITOTIC SPINDLE	62	47	60	**29**	PLK1, CDC42BPA, SYNPO, TOP2A, RACGAP1, YWHAE, TTK, WASF1, ESPL1, CDC42EP1, ALS2, CEP72, KIF15, PCGF5, BUB1, PAFAH1B1, CENPE, ACTN4, CKAP5, NEK2, TPX2, SORBS2, KIF2C, KIF11, KIF4A, KIF23, CCNB2, PREX1, NIN
G2M CHECKPOINT	66	59	38	**6**	MCM6, CDC7, CDC6, MCM2, BARD1, STMN1
E2F TARGETS	67	73	50	**12**	LBR, TIMELESS, RNASEH2A, MCM2, UBE2T, EXOSC8, TK1, RBBP7, MCM7, MCM6, STMN1, BARD1
MYC TARGETS V2	9	16	10	**2**	MYC, NOLC1
P53 PATHWAY	48	47	46	**17**	HDAC3, H2AFJ, ABCC5, DDB2, IRAK1, NDRG1, BTG2, KLF4, HSPA4L, FBXW7, FGF13, RAP2B, IFI30, TSC22D1, ZBTB16, FDXR, JAG2
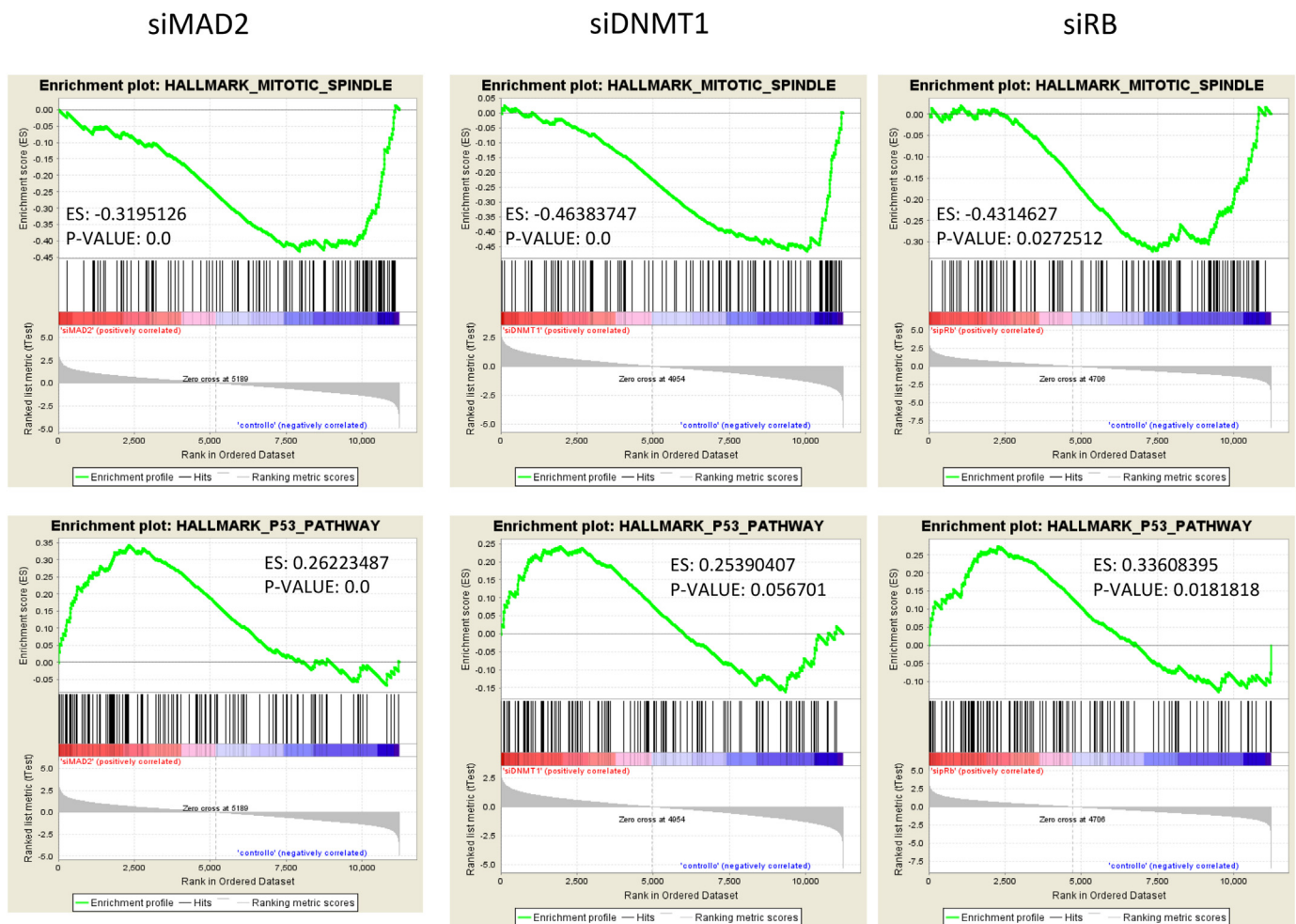
Fig. 6. Significantly enriched GSEA signatures shared by the samples. Enrichment plots of expression signatures of Hallmark gene sets for transcriptional changes in IMR90 cells when treated with RB, MAD2 and DNMT1 specific siRNAs in respect to siGFP control.

than of individual gene(s).

Furthermore, we compared our list of common genes (ANEU66) emerged from the GSEA analysis with similar previously published analyses (Supplementary material S4). From this comparison only 11 genes were shared between our gene list (ANEU66) and the CIN70 list [7], and only one gene was in common with the reported Microsatellite Instability Gene Set (https://amp.pharm.mssm.edu/Harmonizome/gene_set/Microsatellite + Instability/HuGE + Navigator + Gene-Phenotype + Associations).

The constructed PPI network based on STRING included 62 proteins (nodes) and 226 interactions (edges). There were five DEGs with a degree ≥15, among them TOP2A and KIF4A were regarded as hub genes and may be important in aneuploidy establishment. These two genes have been reported to be associated with cancer development. The protein encoded by the TOP2A gene (TopoIIα) is a highly conserved enzyme that catalyzes the ATP-dependent transport of one intact DNA double helix through another. Previous studies have revealed the important role of TopoIIα activity in chromosome segregation. Drugs that interfere with TopoIIα have been reported to induce polyploidy and endoreduplication to different degrees, providing indirect evidence that this enzyme is required for the separation of sister chromatids [37]. Furthermore, perturbation of TopoIIα activity prevents decatenation and disentanglement of the chromosomes and leads to activation of the decatenation checkpoint, which delays progression of G2 cells into mitosis [38]. The KIF4A gene encodes the protein Kif4a, a member of the kinesin superfamily. Several studies have confirmed that the kinesin superfamily is implicated in the regulation of several cellular processes

like the establishment or stabilization of the central spindle, mitotic spindle pole separation during prometaphase and anaphase, and chromatid motility [39]. Kif4a affects chromosome congression and cytokinesis and can also control microtubule dynamics during anaphase and telophase, all of which are involved in proper spindle midzone formation [40].

4. Concluding remarks

By our microarray analyses we identify an 'early aneuploidy" gene expression signature consisting of common genes/pathways that were up- or downregulated in human primary fibroblasts becoming aneuploid by posttranscriptional silencing of a single gene.

Aneuploidy is a hallmark of solid tumors and it is often associated with poor prognosis and oincreased resistance to chemotherapy. Thus, some of the pathways and genes that we found deregulated in aneuploid human fibroblasts might be involved in the malignant transformation. Indeed, several of the identified altered genes have been already linked to cancer phenotype.

Additional work is needed to establish whether our ANEU66 list of genes is recurrent in aneuploid tumors. This would reveal aneuploid-specific targets to be exploited in cancer therapy. Moreover, the molecular pathways generally activated by aneuploidy need to be dissected more deeply. All together this knowledge will pave the way for more precise targeting of aneuploidy with a therapeutic benefit.
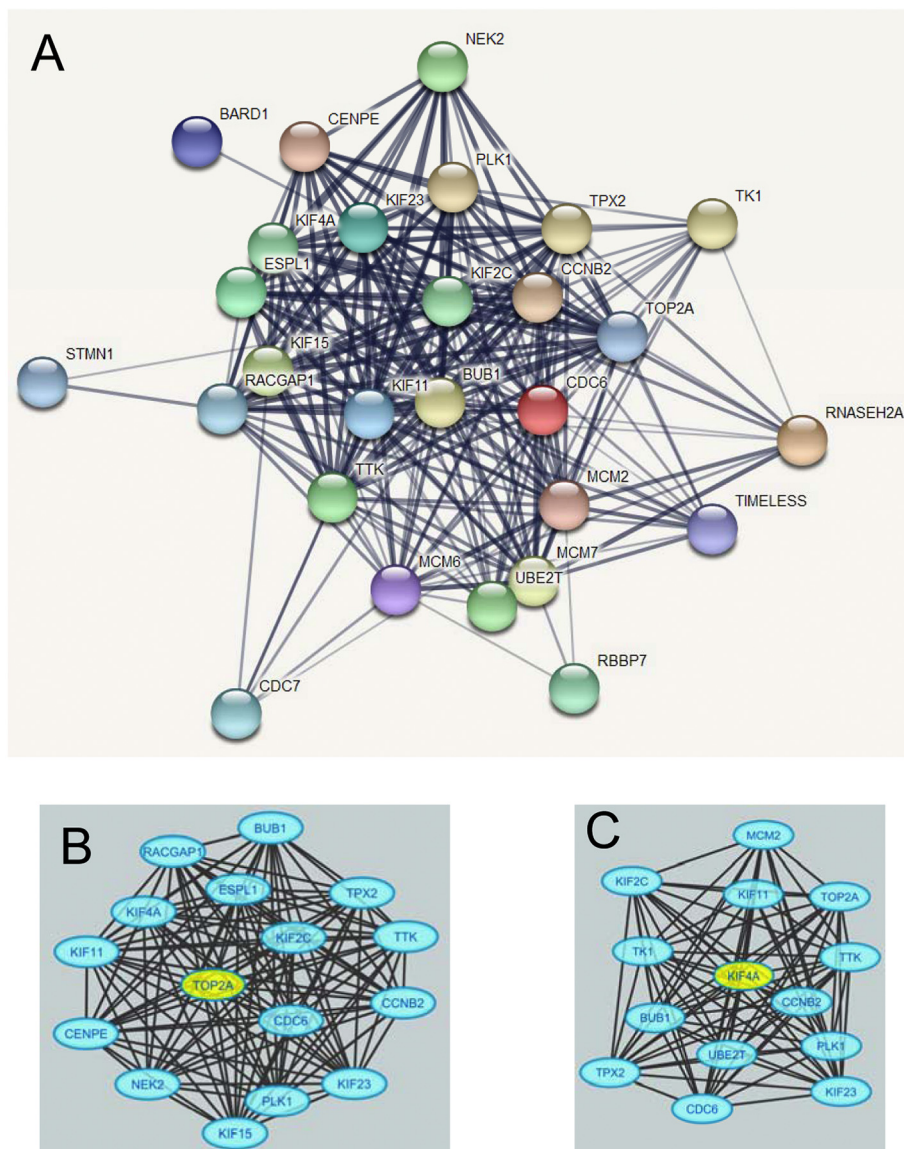
Fig. 7. Protein-protein interaction (PPI) network of DEGs. (A) PPI based on STRING. The network contained 62 nodes and 226 edges. There were five genes edges ≥15: TOP2A (21 edges), KIF2C (18 edges), KIF4A (18 edges), RACGAP1 (18 edges) and TTK (16 edges). (B and C) Modules identified from the network based on STRING. Two modules were identified with $P < 5 \times 10^{-4}$. Module shown in B (nodes, 16; density, 0.361; quality, 0.580; p-value $= 1.319 \times 10^{-7}$) and module shown in C (nodes, 14; density, 0.291; quality, 0.453; p-value $= 7.759 \times 10^{-7}$).

5. Material and methods

5.1. Cells and culture conditions

Primary Human fibroblasts (IMR90, ATCC), characterized by a chromosome number of 46, were cultured in DMEM medium supplemented with 10% foetal calf serum, 100 U/mL penicillin, 100 μg/mLStreptomycin and 1 mM Sodium Pyruvate (all from Gibco, Life Technology, Italy). All cells were maintained at 37 °C under 5% CO_2 and atmospheric oxygen.

5.2. Cytogenetics

Cells were treated with 0.2 μg/mL of colcemid (Demecolcine, SIGMA-Aldrich, Italy) for 4 h, trypsinized and harvested by centrifugation at 1000 rpm for 10 min. Cells were swollen by adding 75 mM KCl dropwise and incubated at 37 °C for 10 min, then centrifuged at 800 rpm for 10 min. The pellet was resuspended adding dropwise 5 mL of cold Carnoy's fixative [methanol/acetic acid (3:1 v/

v)] and incubated for 15 min on ice. After repeating the last step twice, cells were dropped onto iced slides. The slides were air-dried and stained with 3% GIEMSA a in phosphate-buffered saline for 10 min. Chromosome numbers were evaluated using a Zeiss Axioskop microscope under a 100 X objective. We evaluated at least 100 mitoses for each sample. The experiment was repeated twice.

5.3. RNA interference

For siRNAs transfection 2×10^5 cells were plated in 6-well dishes and incubated at 37 °C 1 day before transfection. Specific siRNAs duplexes were mixed with Lipofectamine2000 Reagent (Invitrogen), according to manufacturer's recommendation and added to the cells. After 6 h at 37 °C, the transfection medium was replaced with fresh medium. To silence genes of interest post-transcriptionally, cells were transfected with siRNAs targeting MAD2 (siMAD2: 5'-AUACGGACUCACCUUUtt-3') siRNAs targeting pRB(siRB: 5'-GAAGAAGUAUGAUGUAUUGTT-3') and DNMT1 (siDNMT1: 5'-AUUACGUAAAGAAGAAUUATT-3'), at a final concentration of 60 nM or 80 nM and analyzed at 72 h. A siRNA

targeting the Green-Fluorescent-Protein (siGFP: 5'-GGCUACGUCCAGG AGCGCACCtt-3') at a final concentration of 60 nM was used as a control. All siRNAs (21-nucleotide duplexes) were synthesized by Eurofins-MWG,

5.4. Real-time reverse transcription PCR (RT-qPCR)

Primers to be used in RT-qPCR experiments were designed with Primer Express software (Applied Biosystems, Life Technologies) choosing amplicons of approximately 70–100 bp. The selected sequences were tested against public databases (BLAST) to confirm the identity of the genes. Total RNA was extracted from cells by using the "PureLink RNA mini kit" (Ambion, Thermo Fisher Scientific) according to the manufacture's instruction. RNA was reverse-transcribed in a final volume of 20 μL using the High Capacity cDNA Reverse Transcription kit (Applied Biosystems, Thermo Fisher Scientific) for 10 min at 25 °C and 2 h at 37 °C. For each sample 50 ng of cDNA, was analyzed by RT-qPCR (95 °C for 15 s, 60 °C for 60 s repeated for 40 cycles). RT-qPCR was done in a final volume of 20 μl comprising $1\times$ Master Mix SYBR Green (Applied Biosystems, Thermo Fisher Scientific) and 0.3 μM of forward and reverse primers for: GAPDH (Fw: 5'-CTCATGACCACAGT CCATGCC-3′, Rev.: 5'-GCCATCCACAGTCTTCTGGGT-3′), Rb (Fw: 5'-GCAGTATGCTTCCACCAGGC-3′, Rev.: 5'-AAGGGCTTCGAGGAATGT GAG-3′), DNMT1 (Fw: 5'-GCACCTCATTTGCCGAATACA-3′, Rev.: 5'-TCTCCTGCATCAGCCCAAATA-3′), SERTAD2 (Fw: 5'-CAGGGAACAGT AGGAGCTGG-3′, Rev.: 5'-CGGTTTTCTCGTAAAGGCAC-3′), FAM3C (Fw: 5'-TGGCAAATGGAAAACAGGA-3′, Rev.: 5'-TCAGAAACTCAATAA ATGGTGCC-3′), IGFBP1 (Fw: 5'-GGGACGCCATCAGTACC-3′, Rev.: 5'-CCATTTTTTGATGTTGGTGAC-3′), EGFR (Fw: 5'-CACGCAAACCAGAC CTCAAAG-3′, Rev.: 5'-ACCGCTGCCACTTGTTCTT-3′), NAP1L5 (Fw: 5'-GTCATGTAGCTTTTAGGGTG-3′, Rev.: 5′- GGCACAGCTAATACAAGCA AAC -3′), MARCH4 (Fw: 5'-CTGCTATGGATTGTGTGCCC-3′, Rev.: 5′-AGCGGCACTTGAGGAGAC-3′). Data were analyzed by averaging quadruplicates Ct (cycle threshold). Levels of RNA expression were determined by using the SDS software version (Applied Biosystems) according to the 2-ΔΔct method. Levels of RNA expression of selected genes were normalized to the internal control GAPDH.

5.5. Whole-genome microarrays expression analysis

Total RNA from cells treated with siRNAs for 72 h was extracted using Trizol reagent (Invitrogen) and further purified with RNeasy RNA isolation kit according to manufacturer's instructions (Qiagen; Hilden, Germany). RNA 6000 Nano LabChip kit (Agilent, Santa Clara, CA, USA) was used to determine the concentration, the purity and the integrity of the RNA samples using an Agilent 2100 bioanalyzer. Only samples with a RIN (RNA Integrity Number) > 8.0 were used for analysis. All samples had three independent biological replicates, and each replicate was labeled and hybridized in duplicate with two colour and dye-swap protocol, on a separate array. Cyanine-3 (Cy3) or Cyanine-5 (Cy5) labeled cRNA was prepared from total RNA using the LowInput QuickAmp Labeling Kit according to the manufacturer's instructions (Agilent, Santa Clara, CA, USA). Dye incorporation and cRNA yield were checked with the NanoDrop ND-1000 spectrophotometer (Thermo Fisher Scientific, Waltham, MA, USA). Hybridization and washing were performed using the in-situ Hybridization Plus Kit following the manufacturer's instructions (Agilent protocol: G4140-90050 Gene Expression Two Colour ver. 6.9.1). Briefly, labeled cRNAs was purified using the RNeasy RNA isolation kit (Qiagen, Hilden, Germany) and 1.0 μg of Cy3- or Cy5-labeled cRNA (specific activity > 9.0 pmol Cy/μg cRNA) was fragmented at 60 °C for 30 min in a reaction volume of 55 μl containing $1\times$ fragmentation buffer and $2\times$ blocking agent. On completion of the fragmentation reaction, 55 μl of $2\times$ hybridization buffer was added to the mixture and hybridized to Whole Human Genome Microarray 4x44K (Agilent-G4112F) for 17 h at 65 °C in a rotating hybridization oven. After hybridization, microarrays were washed

1 min. at room temperature with wash buffer1 and 1 min with 37 °C with wash buffer2, then dried immediately. Slides were scanned on the Agilent DNA Microarray Scanner (G2505B) using two colour scan setting for 4x44k array slides (Scan Area 61 × 21.6 mm, Scan resolution 5 μm, dye channels PMT set to 100%). The scanned images were analyzed with Feature Extraction Software 9.5.1, using default parameters (protocol: GE2-v5_95 and Grid: 014850_D_F_20110325) to obtain background subtracted, dye normalized and spatially detrended processed signal intensities. Quality control assessment was performed and two low quality samples (1 siMAD2 and 1 siGFP) were removed from analysis. Raw data of gene expression profiling were submitted to NCBI's Gene Expression Omnibus (GEO) database and can be accessed via accession number GSE120641.

5.6. Gene expression profiling and data analysis

Statistical data analysis, background correction, normalization and summary of expression measure were conducted with GeneSpring GX ver. 12.0 (Agilent, Santa Clara, CA, USA). Data were filtered using two-step procedure: first the entities were filtered based on their flag values P (present) and M (marginal) and then filtered based on their signal intensity values. Statistically significant differences were computed by the Student's *t*-test and the significance level was set at $p < .05$. The false discovery rate (FDR) was applied as a multiple test correction method. Unsupervised hierarchical clustering was performed using the Euclidean distance and the average linkage method. Differentially expressed genes (DEGs) were selected by a supervised approach using the ANOVA package. Formally, a contrast fold change of at least ± 1.5 and an FDR corrected *p*-value < .05 was used in order to perform multiple pairwise comparisons between each class (siDNMT1, siMAD2 and sipRB) and the control (siGFP). DEGs common to all three treatments were subjected to GeneOntology (GO) and biological pathway enrichment analysis using FunRich tool (http://www.oncomine.org/resource/login.html) against human FunRich background database.

5.7. Gene set enrichment analysis (GSEA)

Normalized expression data for all the probe sets obtained from microarray analysis of the siRNA treated IMR90 cells were further analyzed using the Gene Set Enrichment Analysis (GSEA) method [41]. GSEA is a computational method that determines if a priori defined set of genes indicates statistically significant between two phenotypes. In GSEA, genes are ranked by their correlation with phenotype and every enrichment gene set will get an enrichment score (ES). 1000 gene permutations were used to generate a null distribution for ES, then each pathway will attain a normalization enrichment score (NES). H: Hallmark and C5:BP:GO biological process, including 4486 gene sets, were used as gene sets database. Gene sets were considered significantly enriched with *q*-value < 0.1 and *p*-value < .005.

5.8. Protein-protein interaction (PPI) network construction and module selection

A PPI network was constructed based on Search Tool for the Retrieval of Interacting Genes/Proteins (STRING ver. 11.0; https://string-db.org). The DEGs were mapped to STRING networks and PPI pairs were acquired. Interactions with a confidence score > 0.4 were retained in the network and were visualized using Cytoscape (version 3.4.0; http://cytoscape.org/). In the PPI network, a node represents a protein product of a DEG and the edges represents the number of proteins linked to this node. The nodes with a high number of edges (> 15) were considered to be important in the present study. The PPI modules were screened using the ClusterONE plugin (ver. 1.0; http://www.paccanarolab.org/clusterone) in Cytoscape (https://cytoscape.org). Results were considered statistically significant with a *p*-value < .0005.

Acknowledgements

Authors contribution

DC did Western Blot, RNAi experiments, cytogenetics analysis, RT-qPCR, analyzed the bioinformatics data and helped to write the manuscript. SB, FC and SS prepared the samples and made the micro-array experiments. CC made the bioinformatics study of the microarray data. VB analyzed the data, made the figures and helped to write the manuscript. SF Analyzed bioinformatics data and wrote the manuscript. ADL designed the experiments, analyzed the data and wrote the manuscript.

Appendix A. Supplementary data

Supplementary data to this article can be found online at https://doi.org/10.1016/j.ygeno.2020.02.006.

References

[1] N.K. Chunduri, Z. Storchová, The diverse consequences of aneuploidy, Nat. Cell Biol. 21 (2019) 54–62.

[2] K.M. Schukken, F. Foijer, CIN and aneuploidy: different concepts, different consequences, BioEssays 40 (2018) 1700147.

[3] B.A.A. Weaver, D.W. Cleveland, The role of aneuploidy in promoting and suppressing tumors, J. Cell Biol. 185 (2009) 935–937.

[4] S.L. Thompson, D.A. Compton, Examining the link between chromosomal instability and aneuploidy in human cells, J. Cell Biol. 180 (2008) 665–672.

[5] E.M. Torres, et al., Effects of aneuploidy on cellular physiology and cell division in haploid yeast, Science (80-.) 317 (2007) 916–924.

[6] E.M. Torres, B.R. Williams, A. Amon, Aneuploidy: cells losing their balance, Genetics 179 (2008) 737–746.

[7] J.M. Sheltzer, A transcriptional and metabolic signature of primary aneuploidy is present in chromosomally unstable cancer cells and informs clinical prognosis, Cancer Res. 73 (2013) 6401–6412.

[8] M. Dürrbaum, et al., Unique features of the transcriptional response to model aneuploidy in human cells, BMC Genomics 15 (2014) 139.

[9] B.R. Williams, et al., Aneuploidy affects proliferation and spontaneous immortalization in mammalian cells, Science 322 (2008) 703–709.

[10] N. Dephoure, et al., Quantitative proteomic analysis reveals posttranslational responses to aneuploidy in yeast, Elife 3 (2014) e03023.

[11] N. Pavelka, et al., Aneuploidy confers quantitative proteome changes and phenotypic variation in budding yeast, Nature 468 (2010) 321–325.

[12] J.M. Sheltzer, E.M. Torres, M.J. Dunham, A. Amon, Transcriptional consequences of aneuploidy, Proc. Natl. Acad. Sci. 109 (2012) 12644–12649.

[13] C. Viganó, et al., Quantitative proteomic and phosphoproteomic comparison of human colon cancer DLD-1 cells differing in ploidy and chromosome stability, Mol. Biol. Cell 29 (2018) 1031–1047.

[14] F. Foijer, et al., Chromosome instability induced by Mps1 and p53 mutation generates aggressive lymphomas exhibiting aneuploidy-induced stress, Proc. Natl. Acad. Sci. U. S. A. 111 (2014) 13427–13432.

[15] E.M. Torres, et al., Identification of aneuploidy-tolerating mutations, Cell 143 (2010) 71–83.

[16] N. Donnelly, V. Passerini, M. Dürrbaum, S. Stingele, Z. Storchová, HSF 1 deficiency and impaired HSP 90-dependent protein folding are hallmarks of aneuploid human cells, EMBO J. 33 (2014) 2374–2387.

[17] S. Stingele, et al., Global analysis of genome, transcriptome and proteome reveals the response to aneuploidy in human cells, Mol. Syst. Biol. 8 (2012) 608.

[18] S.L. Thompson, D. a Compton, Proliferation of aneuploid human cells is limited by a p53-dependent mechanism, J. Cell Biol. 188 (2010) 369–381.

[19] L. Lentini, V. Barra, T. Schillaci, A. Di Leonardo, MAD2 depletion triggers premature cellular senescence in human primary fibroblasts by activating a P53 pathway preventing aneuploid cells propagation, J. Cell. Physiol. 227 (2012) 3324–3332.

[20] L. Veneziano, V. Barra, L. Lentini, S. Spatafora, A. Di Leonardo, p14ARF prevents proliferation of aneuploid cells by inducing p53-dependent apoptosis, J. Cell. Physiol. 231 (2016) 336–344.

[21] A. Valind, Y. Jin, D. Gisselsson, Elevated tolerance to aneuploidy in cancer cells: estimating the fitness effects of chromosome number alterations by in silico modelling of somatic genome evolution, PLoS One 8 (2013).

[22] A. Amato, L. Lentini, T. Schillaci, F. Iovino, A. Di Leonardo, RNAi mediated acute depletion of retinoblastoma protein (pRb) promotes aneuploidy in human primary cells via micronuclei formation, BMC Cell Biol. 10 (2009) 79.

[23] V. Barra, T. Schillaci, L. Lentini, G. Costa, A. Di Leonardo, Bypass of cell cycle arrest induced by transient DNMT1 post-transcriptional silencing triggers aneuploidy in human cells, Cell Div. 7 (2012) 2.

[24] L.S. Michel, et al., MAD2 haplo-insufficiency causes premature anaphase and chromosome instability in mammalian cells, Nature 409 (2001) 355–359.

[25] G.A. Andriani, E. Maggi, D. Piqué, et al., A direct comparison of interphase FISH versus low-coverage single cell sequencing to detect aneuploidy reveals respective strengths and weaknesses, Sci. Rep. 9 (2019) 10508.

[26] M. Pathan, et al., FunRich: an open access standalone functional enrichment and interaction network analysis tool, Proteomics 15 (2015) 2597–2601.

[27] L. Yuniati, B. Scheijen, L.T. van der Meer, F.N. van Leeuwen, Tumor suppressors BTG1 and BTG2: beyond growth control, J. Cell. Physiol. 234 (2019) 5379–5389.

[28] S. Hanks, et al., Constitutional aneuploidy and cancer predisposition caused by biallelic mutations in BUB1B, Nat. Genet. 36 (2004) 1159–1161.

[29] B.A.A. Weaver, A.D. Silk, C. Montagna, P. Verdier-Pinard, D.W. Cleveland, Aneuploidy acts both oncogenically and as a tumor suppressor, Cancer Cell 11 (2007) 25–36.

[30] V. Coppola, et al., BTG2 loss and miR-21 upregulation contribute to prostate cell transformation by inducing luminal markers expression and epithelial-mesenchymal transition, Oncogene 32 (2013) 1843–1853.

[31] A. Ohashi, et al., Aneuploidy generates proteotoxic stress and DNA damage concurrently with p53-mediated post-mitotic apoptosis in SAC-impaired cells, Nat. Commun. 6 (2015) 1–16.

[32] G.T. Maine, P. Sinha, B.K. Tye, Mutants of *S. cerevisiae* defective in the maintenance of minichromosomes, Genetics 106 (3) (1984 Mar) 365–385.

[33] V. Passerini, et al., The presence of extra chromosomes leads to genomic instability, Nat. Commun. 7 (2016).

[34] S. Santaguida, et al., Chromosome mis-segregation generates cell- cycle-arrested cells with complex karyotypes that are eliminated by the immune system, Dev. Cell 41 (2017) 638–651.

[35] H.Y. Yamada, G. Kumar, Y. Zhang, E. Rubin, S. Lightfoot, W. Dai, C.V. Rao, Systemic chromosome instability in Shugoshin-1 mice resulted in compromised glutathione pathway, activation of Wnt signaling and defects in immune system in *the lung*, Oncogenesis 5 (8) (2016 Aug 15) e256.

[36] C.V. Rao, S. Sanghera, Y. Zhang, L. Biddick, A. Reddy, S. Lightfoot, N.B. Janakiram, A. Mohammed, W. Dai, H.Y. Yamada, Systemic chromosome instability resulted in colonic transcriptomic changes in metabolic, proliferation, and stem cell regulators in Sgo1 − / + mice, Cancer Res. 76 (3) (2016 Feb 1) 630–642.

[37] D.J. Clarke, A.C. Vas, C.A. Andrews, L.A. Díaz-Martínez, J.F. Giménez-Abián, Topoisomerase II checkpoints: universal mechanisms that regulate mitosis, Cell Cycle 5 (2006) 1925–1928.

[38] J.J. Bower, et al., Topoisomerase IIα maintains genomic stability through decatenation G2 checkpoint signaling, Oncogene 29 (2010) 4787–4799.

[39] H. Bringmann, et al., A kinesin-like motor inhibits microtubule dynamic instability, Science (80-.) (2004), https://doi.org/10.1126/science.1094838.

[40] C.K. Hu, M. Coughlin, C.M. Field, T.J. Mitchison, KIF4 regulates midzone length during cytokinesis, Curr. Biol. 21 (2011) 815–824.

[41] A. Subramanian. P. Tamayo, V. Mootha, GSEA: gene set enrichment analysis gene set enrichment analysis: a knowledge-based approach for interpreting genome-wide expression profiles, Proc. Natl. Acad. Sci. U. S. A. 102 (2014) 15545–15550.